### Title

External Measurement of Swallowed Volume During Exercise Enabled by Stretchable Derivatives of PEDOT:PSS, Graphene, Metallic Nanoparticles, and Machine Learning




### Journal

Advanced Sensor Research, 2(4)



### Authors

Polat, Beril
Rafeedi, Tarek
Becerra, Laura L.
et al.



### Publication Date

2023-01-18

Peer reviewed

ADVANCED SENSOR RESEARCH Open Access
www.advsensorres.com

# External Measurement of Swallowed Volume During Exercise Enabled by Stretchable Derivatives of PEDOT:PSS, Graphene, Metallic Nanoparticles, and Machine Learning

*Beril Polat, Tarek Rafeedi, Laura Becerra, Alexander X. Chen, Kuanjung Chiang, Vineel Kaipu, Rachel Blau, Patrick P. Mercier, Chung-Kuan Cheng, and Darren J. Lipomi**

**Epidermal sensors for remote healthcare and performance monitoring require the ability to operate under the effects of bodily motion, heat, and perspiration. Here, the use of purpose-synthesized polymer-based dry electrodes and graphene-based strain gauges to obtain measurements of swallowed volume under typical conditions of exercise is evaluated. The electrodes, composed of the common conductive polymer poly(3,4 ethylenedioxythiophene) (PEDOT) electrostatically bound to poly(styrenesulfonate)-b-poly(poly(ethylene glycol) methyl ether acrylate) (PSS-b-PPEGMEA), collect surface electromyography (sEMG) signals on the submental muscle group, under the chin. Simultaneously, the deformation of the surface of the skin is measured using strain gauges comprising single-layer graphene supporting subcontinuous coverage of gold and a highly plasticized composite containing PEDOT:PSS. Together, these materials permit high stretchability, high resolution, and resistance to sweat. A custom printed circuit board (PCB) allows this multicomponent system to acquire strain and sEMG data wirelessly. This sensor platform is tested on the swallowing activity of a cohort of 10 subjects while walking or cycling on a stationary bike. Using a machine learning (ML) model, it is possible to predict swallowed volume with absolute errors of 36% for walking and 43% for cycling.**

## 1. Introduction

Swallowing is a critical step in bodily nutrition and hydration. Healthy individuals perform 500–700 swallows per day and are generally unaware of its physiological intricacy. Most devices for the assessment of swallowing function available in the literature are intended to detect dysphagia—an ailment that afflicts many survivors of throat trauma and neck cancer.[1–8] For such applications, there is a need to supplement or replace invasive exams designed to assess swallowing function (e.g., videofluoroscopy, endoscopy, and palpation) performed by specialized healthcare professionals.[9–13] Wearable sensors for measuring swallowing signals can also find applications in the study of behavior related to nutrition and hydration. Continuous and mobile monitoring of eating and drinking could be a critical aid to understanding eating disorders and monitoring of adherence to a prescribed diet.[14–16] For example, monitoring intake of water during exercise would be integral to assessing hydration. Currently, there are very few mobile technologies that evaluate swallowing function that have been shown to work under the conditions of exercise. In this work, we developed a mobile platform for the estimation of swallowed volume using a wearable patch (**Figure 1**). The patch is enabled by purpose-synthesized conductive polymers for surface electromyography (sEMG) sensors, graphene sensors for measuring the movement of the skin while swallowing, and an a machine learning (ML) algorithm for estimating swallowed volume from the data extracted with these sensors. Critically, the robust polymeric materials, along with ML, permit this platform to negotiate the effects of motion even in the presence of sweat.

Normal swallowing involves the coordinated movements of a range of structures in the head and neck, which propel a solid or liquid bolus from the oral cavity to the esophagus. The physiological stages of swallowing are described in detail using well-established models such as the Four Stage Model.[17] In brief, after ingestion of a bolus, the submental muscles contract bringing the larynx upward to meet the epiglottis. This action

B. Polat, T. Rafeedi, L. Becerra, A. X. Chen, R. Blau, D. J. Lipomi
Department of NanoEngineering and Chemical Engineering Program
University of California
9500 Gilman Drive, Mail Code 0448, La Jolla, CA 92093-0448, USA
E-mail: dlipomi@eng.ucsd.edu
L. Becerra, K. Chiang, C.-K. Cheng
Department of Computer Science and Engineering
University of California
9500 Gilman Drive, Mail Code 0404, La Jolla, CA 92093-0404, USA
V. Kaipu, P. P. Mercier
Department of Electrical and Computer Engineering
University of California
9500 Gilman Drive, Mail Code 0407, La Jolla, CA 92093-0407, USA

The ORCID identification number(s) for the author(s) of this article can be found under https://doi.org/10.1002/adsr.202200060



**DOI: 10.1002/adsr.202200060**

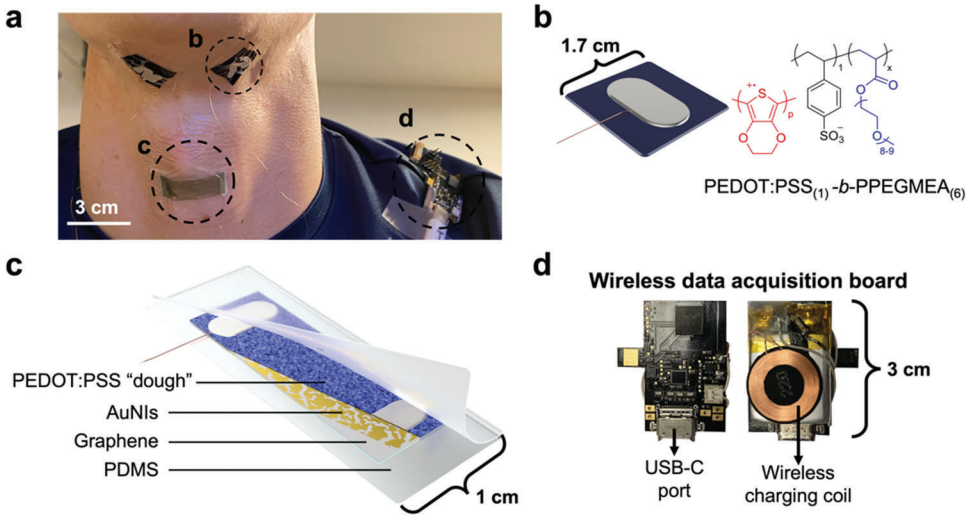


**Figure 1.** Schematic explaining the components of the wireless sensor system. a) The placement of the sEMG and the strain gauges on the neck of a participant. b) Schematic drawing and the chemical formula of the PEDOT:PSS$_{(1)}$-*b*-PPEGMEA$_{(6)}$ (Block-6) sEMG electrode. c) A layer-by-layer schematic of the piezoresistive Gr/AuNI/PEDOT:PSS "dough" strain gauge. d) The front and back side photographs of the wireless PCB board.

allows the bolus to enter the esophagus toward the stomach.[17–22] Many assessment methods for swallowing focus on two stages of this process: the oral propulsion and the pharyngeal stages. These two stages occur almost concurrently for a liquid bolus swallow. Each step of the process produces distinctive electrical signals arising from the neuromuscular activity. Additionally, concomitant tensile deformation of the overlying skin during a swallow generates signals that can be measured epidermally. One of the first sensing modalities used for swallow assessment (for discerning dysfunction) was needle-based intramuscular EMG and/or sEMG.[23–25] Due to its non-invasiveness, sEMG is generally preferred over its transdermal counterpart. Conventionally for sEMG, silver/silver chloride (Ag/AgCl) is used as the electrode material along with a conductive ionic gel that helps decrease the electrode-skin impedance at the interface. Although the use of commercial Ag/AgCl is still predominant in clinical settings, there has been a shift in research laboratories from gel electrodes to dry electrodes.[26] Specifically, dry contact electrodes based on thin metal films[27,28] (such as gold), ionic liquids,[29] and intrinsically conductive polymers[30–34] are becoming increasingly popular for acquiring epidermal biopotential signals. Their skin conformability, stretchability, and longevity ensure better electrical contact over the time of use.

A common base polymer used for dry sEMG electrodes is PEDOT:PSS. Electrodes made only with PEDOT:PSS, although sufficiently conductive, tend to be brittle and unconformable. To address these mechanical limitations, it is often combined with plasticizers and other polymeric additives. For example, Zhang et al. demonstrated a polymer-based electrode composed of a PEDOT:PSS, waterborne polyurethane, and D-sorbitol.[33] The authors demonstrated that the adhesive force of the electrode was significantly enhanced when contacted with wet skin without compromising the electronic properties. Similarly, Cao et al. found a blend of PEDOT:PSS, poly(vinyl alcohol) (PVA), and tannic acid to be an effective dry ECG/EMG electrode with resistance to sweat.[35] However, in such blends, small molecules tend to leach from the polymer matrix over time hence compromising its function. A common advantage to using conductive polymers is that they are usually solution processable. Fabricating electrodes from solvated polymer simplifies the incorporation of additives and allows for the molding of customized geometries. As an example, Wang et al. used PEDOT:PSS as a conformal coating in the fabrication of a stretchable concentric biopotential electrode.[32] The authors achieved an improved interfacial conductivity which was due to the addition of PEDOT:PSS and the spatial filtering geometry (concentric ring), showing superior noise reduction when compared to various electrodes from the literature. Similarly, Zhao et al. coated a graphene layer with modified PEDOT:PSS (with sodium dodecyl sulfate and bis(trifluoromethane) sulfonimide lithium salt) and transferred it onto an elastomeric substrate to use as an sEMG sensor. They also demonstrated good conformability with the skin and electrical properties over the long term.[34]

Even though sEMG has been used in a myriad of wearable and mobile devices for the detection of muscle activation, the biopotential signals can still be distorted due to movement artifacts, electromagnetic noise, crosstalk, and internal noise.[36,37] Much of this noise can be minimized by using shielded cables and achieving good conformability with the skin. Conformability and reliable adhesion reduce any undesired electrode motion thus reducing mechanical noise from the electrode. To attenuate the internal and electromagnetic noise (60 Hz power–line interference), a high pass filter and a notch filter can be used, respectively. However, coping with noise due to the motion of a human subject is more difficult to address in terms of both robustness of wearable devices over time and post-processing of the signal. When commercial Ag/AgCl sEMG electrodes were used, we observed the lifetime of the electrodes to be no more than 60 min before they lost their stickiness while exercising. Our choice of intrinsically conductive and stretchable Block-6 as the sEMG electrode aims to address these difficulties. The superior conformability and durability of Block-6 on the skin allowed for detection of

sEMG signals with reduced motion artifacts, for prolonged sessions, and under conditions of perspiration.

Along with sEMG, orthogonal modalities of sensing such as sound, pressure, bioimpedance, and strain recordings are also used to correlate mechanical motion with muscle activation.[38–46] Specifically, epidermal strain gauges placed on the submental region can detect the movement of the swallowing structures during a swallow. For example, Kim et al. developed a gold film-based sEMG electrodes as well as a commercial piezoresistive strain gauge printed on a conductive adhesive epoxy for detection of laryngeal motion.[38] This method outperformed a nasal cannula in the clarity of the signal. Moreover, the mechanical activity of the throat is often monitored using noncompliant devices such as microphones,[47] accelerometers,[48] and nasal cannulas.[48] Research on epidermal strain gauges, however, has spawned promising compliant and novel materials for such applications. A common approach seen in literature is the use of nanoparticle fillers to impart piezoresistive properties on a host or substrate of soft polymer. Conductive fillers such as silver nanowires, copper nanowires, or carbon nanotubes can be used to modulate the piezoresistivity of polymer hosts such as conductive PEDOT:PSS and insulating polyurethane (PU) and polydimethylsiloxane (PDMS).[41,42,45,46] Ionic liquids and liquid metal alloys have also been used as the active components of swallowing sensors.[43,49] Previously, our group described a strain gauge based on monolayer graphene decorated with metallic nanoislands that when combined with an ML algorithm, was able to detect swallowing differences between healthy and dysphagic patients.[39] It was also able to distinguish different types of boluses based on their mechanical properties. This system exhibited high sensitivity at a low strain regime, however, failed above 2% strain. Our group later incorporated highly plasticized PEDOT:PSS into the sensor complex to increase the range of reversible sensing to 86% strain.[50] A similar sensor fabrication was featured in our most recent work on swallow volume ML prediction.[51] During these experiments, the participants were seated in a relaxed position and the sensors were directly wired to a data acquisition system. However, the described system was unequipped mechanically or electronically to handle the exercise conditions examined in this paper.

With the increased acceptance of remote and wearable medical technology, the need for robust wireless sensing and data acquisition becomes more pressing. For that, enhancements are needed in several areas including the form factor of the wearable devices, the filtering of unwanted motion artifacts caused by movement, and the incorporation of advanced data analysis tools. In this paper, we demonstrate the design and fabrication of such a system with materials-enabled strain and sEMG sensors that interface with a wireless data aquisition PCB. We also train and test a swallow-volume classificationML model to analyze the data from participants ingesting different volumes of water while exercising. Our strain gauge was made up of Gr/AuNIs/PEDOT:PSS nanocomposite allowing it to detect minute differences between distinct swallowed water volumes . Unlike many other reported devices in literature, where the sensors are made of rigid materials, our strain sensor is amenable to stretching with the skin's changing topography. Similarly, our Block-6 based sEMG sensor showed good conformability and longevity on the skin over the period of an hour. We also designed and utilized a wireless data acquisition to conduct swallowing experiments under non-stationary conditions to prove the performance of this sensor platform and the ML predictions for each swallowed water volume.

## 2. Experimental Design

### 2.1. Nanocomposite Strain Gauge

The strain gauge comprising a monolayer of graphene (Gr) with thermally evaporated gold nanoislands (AuNIs) on top (thickness 8 nm) was made following a procedure described in our earlier work.[51,39,50] The choice to use this strain gauge was made due to its well-described high sensitivity and resolution at small strains (up to 2%) and its near-zero temperature coefficient of resistance.[52,53] The Gr/AuNIs composition exhibits a gauge factor of ≈17 at 10 ppm and a gauge factor ≈125 at 1 ppm when the metallic nanoislands form a percolated network (nominal thickness <10 nm).[52] This resolution is due to the combination of piezoresistive properties of both graphene and the ultrathin gold film. Monolayer graphene has piezoresistive properties due to its electronic band structure and the electron scattering caused by the defect points in the film.[54–58] The AuNIs exhibit piezoresistive properties owing to the nanoscale cracks imparted by mechanical stress.[52] Another advantage of the Gr/AuNIs film comes from the ability to tune the ratios of graphene and metal to achieve a near-zero temperature coefficient of resistance; this property makes it amenable to devices intended to be worn in diverse environments.[53] In order to increase the dynamic strain range of the sensor (up to 86%) and improve its robustness, we spray-coated the Gr/AuNIs with a highly plasticized PEDOT:PSS conductive polymer (PEDOT:PSS "dough").[59] The addition of the plasticized conductive polymer provided an alternate pathway for electron transport to compensate for local fractures on the Gr/AuNIs, and thus increased the dynamic range of strain over which a reproducible response could be measured.[50] Electrical insulation from the skin was established by sandwiching the sensor film and the wiring with two spin-coated films of polydimethylsiloxane (PDMS) as illustrated in Figure 1.

### 2.2. Conductive Polymer-Based sEMG Sensor

The sEMG electrodes were made using PEDOT:PSS$_{(1)}$-*b*-PPEGMEA$_{(6)}$ block copolymer ("Block-6") designed and synthesized with electrical and mechanical properties tuned for measuring electromyography signals on-body (**Figure 2**).[60] PEDOT:PSS is a conductive polymer used in many different fields of electronics due to its high conductivity with additives and its molecular stability.[61–65] However, the additives used to increase the stretchability and the conductivity tend to be toxic and can leach out over time decreasing the performance of the polymer. Hence, we opted for intrinsically stretchable Block-6 (specifically the 1:6 ratio of PSS to PPEGMEA). We found that films of PEDOT:PSS$_{(1)}$-*b*-PPEGMEA$_{(6)}$ did not dissolve when stored in a water bath for 5 d at room temperature.[60] The mechanical properties of Block-6 (elastic modulus around 9 MPa) were also superb and comparable to human skin.[66] sEMG electrodes for this study were

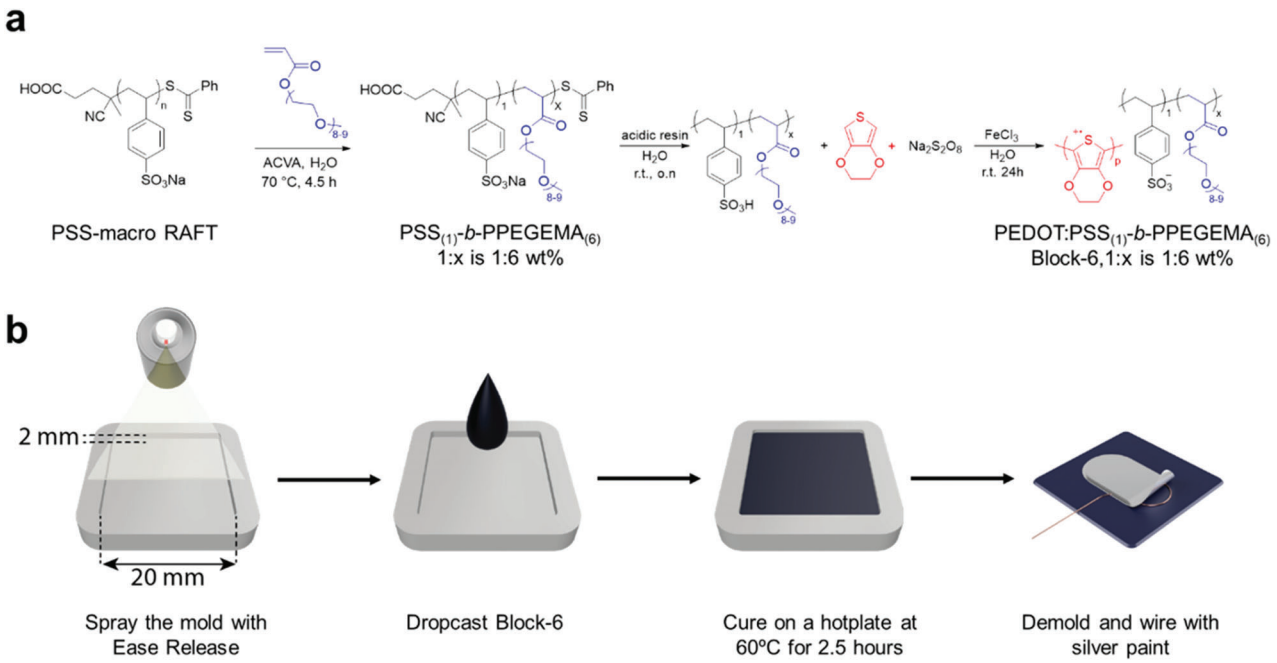


**Figure 2.** A detailed step-by-step fabrication of the Block-6 sEMG sensors. a) The general reaction steps are shown. The procedure was described in an earlier publication.[60] b) The schematic shows the fabrication steps of sEMG electrode films using the synthesized Block-6.

fabricated from drop-cast Block-6 films with the dimensions of 1.7 cm × 1.7 cm. They were dimensioned to fit comfortably on the submandibular region. Mechanical characterization of the films was done by a tensile test until failure. The electrical properties of the material were assessed by the change in resistance over 400 stretching cycles, and electrode impedance on the skin was reported over 1 h.

### 2.3. Human Subject Studies

In our previous work, we demonstrated that the Gr/AuNIs strain gauge and conventional Ag/AgCl (3 M) sEMG sensors can be used to measure different swallowed volumes while the participants were seated. Realistically, patients or athletes would not be using the device when sitting still. Therefore, we designed two scenarios: walking and cycling on a stationary bike while swallowing. We reasoned that participants could be walking around their house while completing their exercises for swallow therapy or could be on their exercise machine to get an insight into their swallowing behavior. We tested volumes between 10–30 mL in 5 mL increments. Anything below 10 mL had worse prediction outcomes in the ML algorithm due to the low amplitude of the signal, as shown in our previous work.[51]

## 3. Statistical Analysis

### 3.1. Processing sEMG and Strain Signals

Raw sEMG and strain data were digitally processed in a sequence of steps in preparation for further analysis. The first step was filtering the raw sEMG and strain data. For the sEMG signals, a 60 Hz notch filter was applied to reduce ambient electrical noise. That was followed by a high pass filter with a 30 Hz cut-off frequency to filter out most of the artifacts since the main frequency of sEMG signals usually ranges from 30 to 250 Hz.[67–69] As for the strain signals, a typical peak lasts around ≈200 ms to 1 s. Therefore, a bandpass filter with a 0.5 Hz low cut-off frequency and a 10 Hz high cut-off frequency was applied. To smooth the data, a third order Savitzky–Golay filter and a 16-sample (0.25 s) moving average were successively applied. These steps ensured easier feature identification in next stage.

### 3.2. Feature Extraction

After the signals were filtered, several of their features were evaluated and extracted using MATLAB to enable the ML analysis. Three sEMG features were extracted out of the processed signals. First was the summation of the peak intensities along the swallowing peak in the sEMG signal. Second was based on the width of the sEMG peak. The width of the sEMG peak was defined as the total length of time when the absolute sEMG signal was above the 99th percentile within the peak. Lastly, the power of the low-frequency components of the sEMG signal. This feature was chosen for its strong correlation with the swallowed volume. The sEMG signals were converted to the frequency-domain with Fast Fourier transform (FFT) to obtain the root mean square (RMS) value between 30 and 100 Hz as the third feature (Figure S1, Supporting Information). For the strain data, two features were extracted from the processed strain signals. The data between $t = 7$ and 12 s were first extracted. Then, local peaks with widths of at least 250 ms and the prominence of at least the quarter of the (max − min) of the signals were identified. The peak closest to $t = 10$ s and the following peak were selected as the peaks of the swallow. The first strain feature was defined as

the peak-to-peak interval between the first and the second peak in the swallow signal. The valley point was further obtained by finding the minimum point between the two peaks. Then the second feature was defined as the difference between the valley point and the middle of the two peaks (which can be viewed as the skew of the peaks). Lastly, an additional feature was defined as the offset between the peak of the sEMG power and the first peak point of the strain signal.

### 3.3. Machine Learning

The correlation between each feature value and the corresponding swallowed volume were visually examined by plotting. The features were normalized to zero mean and unit variance within each data set and then pooled together. Then, the scatter plots for each feature were plotted where the solid-colored lines indicated the mean of each data set, and the thick black line indicated the mean of all samples (Figure 5). We also employed a leave-one-out validation to evaluate the performance of predicting the swallowed volume using the sEMG and strain features previously defined. Within a session, each trial took turns to serve as the testing data, and all the other trials in the session were treated as the training data. An outlier detector was applied to filter out outliers in the training samples which had the $z$-score larger than 2 in any feature dimension. Support vector regression (SVR) model was used to due to the small size of the data set. The SVR model is known to be more robust when the number of feature dimensions is relatively large compared to the number of samples.[70] The prediction model was implemented using Scikit library in Python. After the machine learning analysis was done, the prediction error for each swallowed volume (for walking and cycling) was evaluated according to Equation (S5) in the Supporting Information document.

### 3.4. General Data Processing and Presentation

Sheet resistance measurements were collected using 3 square Block-6 samples, each sample was probed at least 3 times along its width and length (total measurements $n = 18$). The thickness of the samples was taken at 4 measurements per sample (i.e., $n = 12$ for all 3 samples) and the area of each sample was measured once. Tensile testing was done using $n = 3$ Block-6 and $n = 3$ Clevios (PEDOT:PSS) dog-bone samples. The linear regime of each set of data was determined by finding the point at which the coefficient of determination ($R^2$) of each linear regression dropped below 0.98. The corresponding uncertainty in the sheet resistance, thickness, modulus, and toughness was evaluated using the standard deviation. The surfaces conductivity was calculated using Equation (S3) in Supporting Information document provided with its uncertainty based on standard error propagation.

## 4. Results and Discussion

### 4.1. Mechanical and Electrical Properties of Block-6 sEMG Sensors

The results of the mechanical and electrical characteristics of the sEMG sensor films are shown in **Figure 3**. We first compared the electrode-skin impedance spectra of Ag/AgCl (3 M), PEDOT:PSS (Clevios), and Block-6 sEMG sensors over 60 min. Over time, the impedance between the skin and the sensor should stay the same with a slightly decreasing trend due to the secretion of sweat from the skin. Figure 3a shows the initial impedance spectra reading of Block-6, Ag/AgCl, and PEDOT:PSS from 1–$10^5$ Hz range. The impedance values over time at 10 and 100 Hz for Block-6, Ag/AgCl, and PEDOT:PSS are also shown in Figure 3b. The electrode-skin impedance of the Block-6 was 483 kΩ at 10 Hz and 85 kΩ at 100 Hz at the beginning of the experiment. Similarly, we measured the Ag/AgCl electrodes to be 97 kΩ at 10 Hz and 13 kΩ at 100 Hz, and PEDOT:PSS to be 2 MΩ at 10 Hz and 197 kΩ at 100 Hz. After 60 min, we observed the impedance values stayed around the same for all three sensors with a slight decrease toward the end. This decrease in impedance was attributed to the secretion of sweat (includes salts and minerals) from the skin over time. In addition to the impedance spectroscopy, we also measured the average sheet resistance to be $9.4 \pm 3.5$ kΩsq$^{-1}$ and conductivity to be $0.027 \pm 0.022$ Scm$^{-1}$ which was in accordance with the previously published values for Block-6.[60] Calculations of sheet resistance and surface conductivity are included in the Supporting Information.

In comparison to commercial formulations of PEDOT:PSS, Block-6 had a modulus closer to that of skin around the neck ($16 \pm 6$ MPa in comparison to $1.78 \pm 1.73$ MPa[71]), as shown by its tensile response (Figure 3c). Likewise, while commercial PEDOT:PSS was relatively brittle (≈5% fracture strain[60]), Block-6 was both more stretchable (i.e., it has both greater fracture strain at 85% and greater intrinsic elasticity) and tougher (average toughness value at $1.97 \pm 0.25$ MJ m$^{-3}$). Therefore, it was better suited for sensor applications on the skin that were subject to continuous or cyclic strains. Assuming the elastic behavior of Block-6 was Hookean in nature (i.e., in the elastic regime, the change in stress is linear relative to the change in strain), we determined that the linear elasticity of Block-6 was ≈10%. Therefore, we conducted cyclic piezoresistance measurements (400 cycles) from 0% strain up to 5%, 10%, 15%, and 20% strain on the Block-6 films (Figure 3d). Figure 3e shows the full 400 cycles for 5% strain and Figure 3f shows a 10 s window of the same cycles. There was essentially no change in baseline resistance over time with the 5% strain cycle and a slight gradual shift in baseline resistance for the 10%, 15%, and 20% strain cycles (Figure S2, Supporting Information). The gradual shift was due to the plastic deformation of the films above 10% strain, suggesting that the intrinsic elasticity of these Block-6 films was slightly lower than 10% (e.g., closer to 9%). However, the signal generated by the change in strain from cycle to cycle remained distinct and clearly observable, suggesting that the piezoresistive behavior of Block-6 is stable despite constant mechanical deformation and relaxation (Figure S2, Supporting Information).

### 4.2. Results Obtained from Human Subjects

We collected swallow signals for volumes 10, 15, 20, 25, and 30 mL of water under walking and cycling conditions to show that our sensor system was robust enough to distinguish the swallowing event. We asked the participants to walk or bike with the water in their mouth for 10 s and then instructed them to swallow the

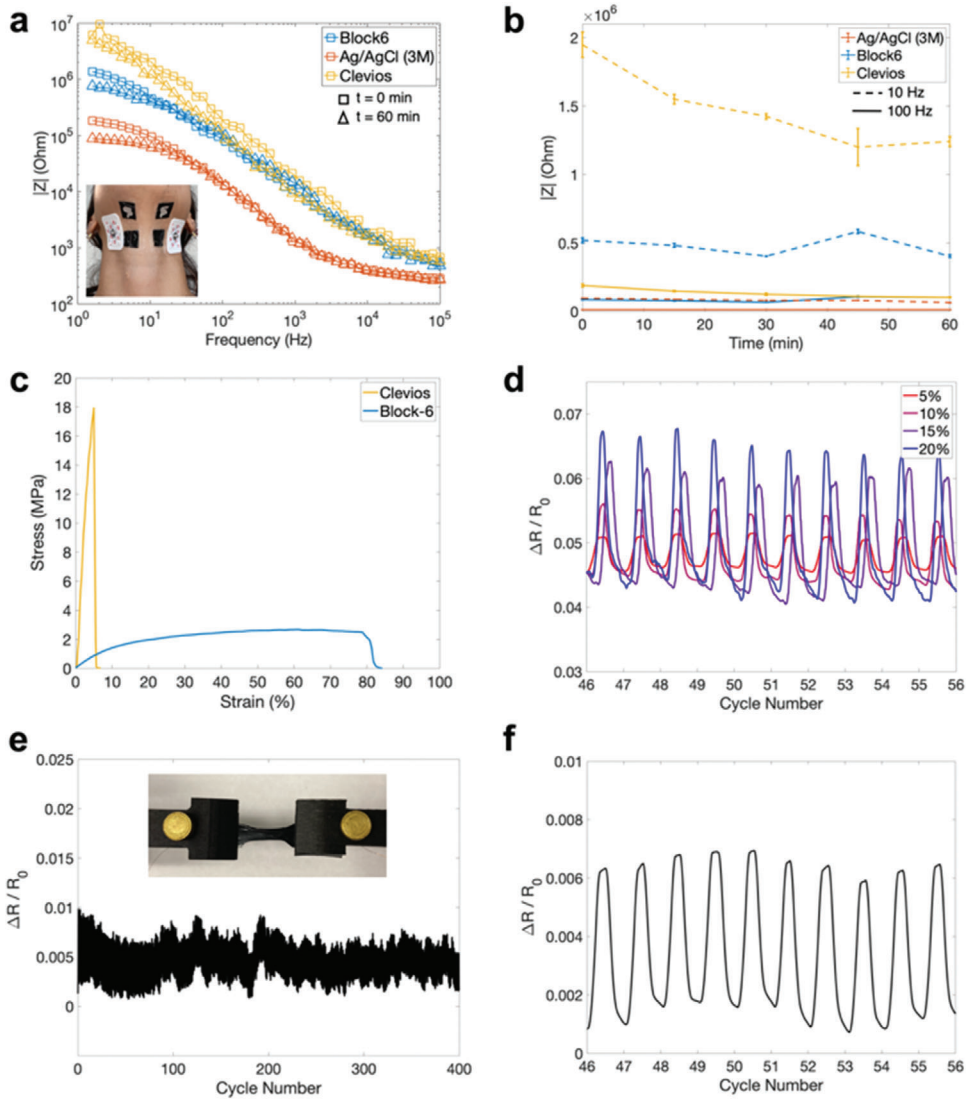


**Figure 3.** Mechanical and electrical characterization of Block-6 sEMG sensor films. a) The plot shows the impedance spectra of Block-6, Ag/AgCl/ (3M) and Clevios on skin over 60 min (square: 0 min, triangle: 60 min) and b) the values at 10 and 100 Hz over time performed on a single subject; measurement was collected 3 time. Impedance measurements with controlled neck placement are in Figure S6 (Supporting Information). c) A representative stress-strain curve of Block-6 and Clevios films are shown. d) Piezoresistive measurements of Block-6 films were measured at different cyclic strains over 400 cycles (shown only for cycles 46–56). e) Plot shows the full 400 cycles of the 5% cyclic strain experiment whereas f) shows the expanded view of the piezoresistive behavior of Block-6 under continuous strain and relaxation.

water and keep on the physical activity until the recording was over. In **Figure 4**a,b, we plotted representative sEMG and strain signals from a 10 mL water swallow while the participant was walking around. Clearly, the raw signals included low-frequency motion artifacts from the body movement in addition to the swallowing muscle contraction however once we processed the signals, we were able to detect the distinct swallow feature from the signal. We calculated the signal-to-noise (SNR) to be 2.78 for the sEMG signals and 2.99 for the strain signals for the walking experiments. Similarly in Figure 4c,d, the motion artifacts were even more prominent in the raw data collected while the participants were cycling but not so much when the data was processed. The calculated SNR for the sEMG signals was 6.94 and 2.63 for the strain signals for the cycling experiments.

### 4.3. Machine Learning Results

Once the collected swallow data were processed, we extracted the features from the swallow peaks in the sEMG and strain signals. From the sEMG signals, we extracted summation, width, and low-frequency power whereas from the strain signals we extracted the peak-to-peak width, peak skew, and the peak offset between the sEMG and the strain (**Figure 5**a,b). Figure 5c shows the correlation between features and the swallowed volumes for all the experiments (Figure S5, Supporting Information shows the correlations for walking and cycling experiments separately). On average, there was a trend between the volumes swallowed and the extracted features. In our results, sEMG summation, and low frequency power showed positive correlation whereas the sEMG

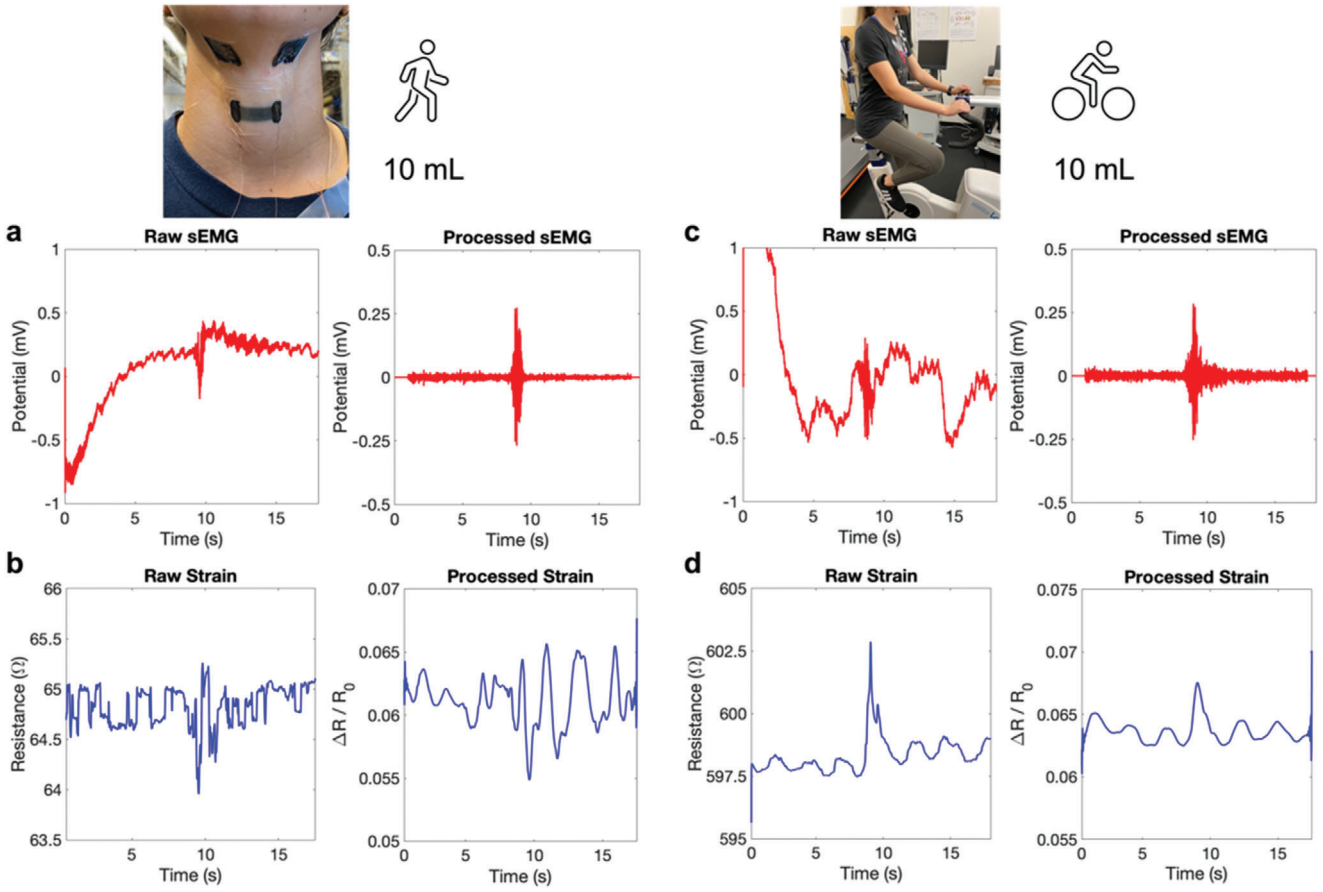


**Figure 4.** Representative processed data of sEMG and strain signals from each type of exercise. Photos show the experimental setup for the swallowing while walking and cycling. Left panel plots show a) of a raw and processed 10 mL swallow sEMG signals and b) strain signals during walking experiments. Right panel plots show raw and processed 10 mL swallow c) sEMG signals and d) strain signals during cycling experiments.

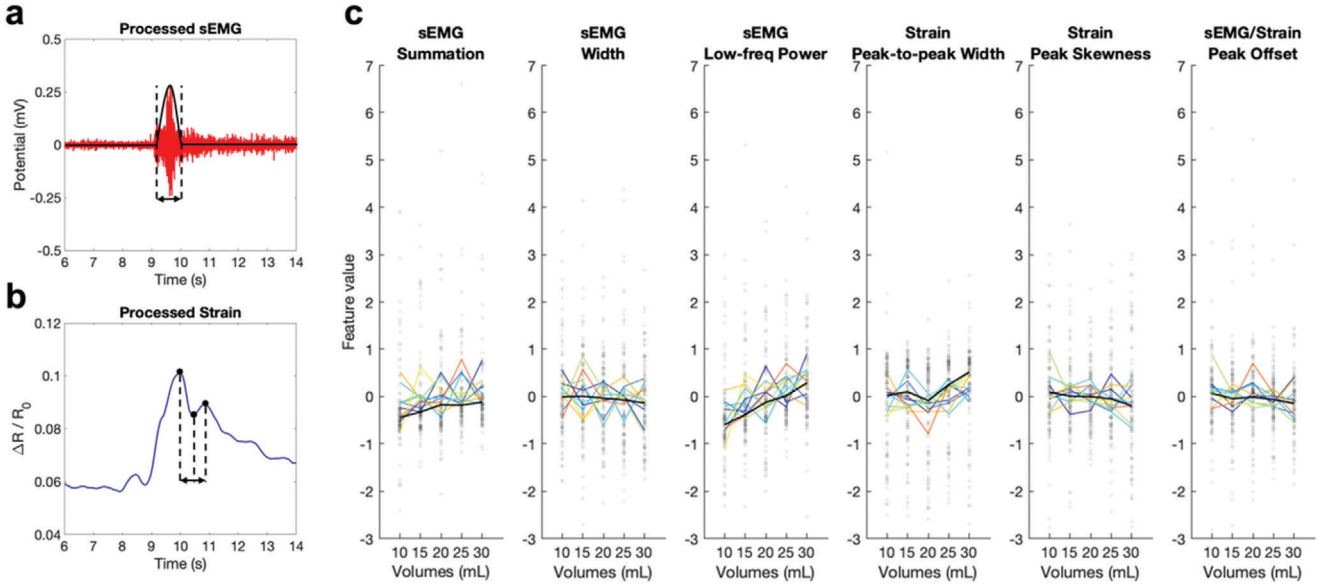


**Figure 5.** The correlation between the volumes and the extracted features for all the walking and cycling experiments. The example plots for a) sEMG and b) strain signals from a swallow show the extracted features. c) The correlation between the swallowed volumes and the extracted features for each participant's data (in color) and the overall average (in black) are shown. The vertical dots represent each trial within a volume for all 10 participants for walking and cycling (10 swallows per volume per experiment).

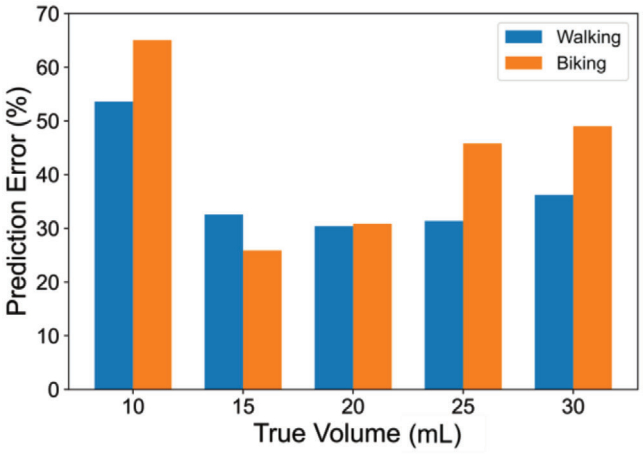


**Figure 6.** ML prediction results. The plot shows the percent error for each volume for the walking and cycling (biking) experiments.

signal width showed a negative correlation. The highest positive correlation was observed in the low frequency power from the sEMG signals. We observed a positive correlation for the peak-to-peak width for the strain signal and negative correlation for the peak skew and the peak offset between the sEMG and strain signals. Due to the low sample size of these experiments, the correlations produced for this model lacked in precision. Nevertheless, we were able to exact the signal features with the best prediction ability for our data to enable further ML analysis.

Lastly, we trained the ML model using these features to predict each swallowed volume. **Figure 6** shows the performance of this prediction model. On average, the predictions of swallowed volume were better for the walking than they were for cycling experiments likey due to the fewer motion artifacts involved(except for the 15 mL). The model also predicted the volumes of intermediate size (15, 20, and 25 mL) with higher accuracy than the smallest (10 mL) and the largest (30 mL). The relative accuracy in predicting these intermediate volumes, when compared to that of the 30 ml, could be due to the observed effort exerted and motions expressed by the participants to hold the 30 mL water swallow it. We also observed large prediction error in swallows of 10 mL. This error could be attributed to the premature and involuntary movement of the liquid bolus from the oral cavity into pharynx that occurs before swallowing smaller volumes causing swallow disruptions (this was also observed in our previous work[51]). Overall, however, the results of the model were promising, as they show that this sensor platform can be used to predict the swallowed volumes even when the participants were moving and sweating.

## 5. Conclusion

In this work, we created a platform capable of collecting sEMG and strain signals from the submandibular area of the neck during a swallow. These data could be wirelessly transferred from a PCB worn by the participant to a phone application, and then processed using an ML algorithm. Both types of sensors were able to resolve features of the swallowing motion that permitted estimation of swallowed volume, even when the participants were exercising. We successfully employed a recently published material (Block-6) as the sEMG sensor in our experiments. The mechanical and electrical properties of Block-6 were superior to conventional PEDOT:PSS (Clevios). These properties allowed Block-6 sEMG sensors to last longer on the skin of the participants skin during the exercise experiments compared to commercial Ag/AgCl electrodes, which delaminated after 60 min. Moreover, potentially toxic additives, that are commonly used with conductive polymers, were not needed to achieve the conductivity and stretchability required for collection of sEMG signals. While we designed this system to measure swallowed volume in contexts such as those in sports medicine, we believe that it embodies the right characteristics for broader use. In the area of dysphagia arising from a range of conditions—neurologic, traumatic, or as a result of radiation therapy—the ability to assess swallowing function using a wearable device can be invaluable. In particular, the use of ML for automatic classification of the data holds considerable potential.

## 6. Experimental Section

*Fabrication of Strain Gauges*: The strain gauges were fabricated by thermal evaporation of gold nanoislands (at 0.03 $Å s^{-1}$ with a nominal thickness of 8 nm) onto a single layer of graphene grown on both sides of a 75 mm × 75 mm copper foil (GrollTex, Inc). The excess graphene layer on the backside was etched in the air plasma cleaner for 5 min at 30 W and 250 mTorr. A 200 nm thick film of 4 wt% poly(methyl methacrylate) (PMMA, Alfa Aesar) dissolved in anisole (Sigma Aldrich) was spin-coated on top of the Gr/AuNIs complex at 4000 rpm for 60 s and annealed on a hotplate at 150 °C for 10 min. The PMMA film acted as a supporting layer for the following water transfer process. The underlying copper foil was etched on top of a 0.05 $gmL^{-1}$ ammonium persulfate solution (APS, Acros Organics). The floating Gr/AuNIs/PMMA film was later transferred onto a tattoo paper spin-coated with polydimethylsiloxane (Sylgard 184 PDMS, 10:1 base-to-curing agent ratio) at 1000 rpm for 60 s and dried completely for 12 h. Once fully dried, the PMMA film was etched away in an acetone bath for 1 min at 50 °C. A PEDOT:PSS "dough" solution was spray-coated on top of the Gr/AuNIs in timed intervals: 8 × 1 s, 4 × 10 s, and 4 × 20 s, with 1 min drying period and rotation of sample 90° after each interval. After the last interval, the sample was dried on a hotplate at 150 °C for 5 min. The copper wiring was attached with silver paint for electrical connection. As the final layer, another PDMS layer (30:1 base-to-curing ratio) was spin-coated on top at 1000 rpm for 60 s and cured for 1 h on a hotplate at 110 °C. At this stage, the strain gauges were ready to be cut out of the substrate and placed on the throat of the participant with the tattoo paper side facing away from the skin.

*Fabrication of sEMG Sensors*: The sEMG sensor films of Block-6 were made by drop-casting in square molds (20 mm × 20 mm × 2 mm depth) that were 3D-printed with Clear V4 resin using FormLabs—Form 3 at 0.025 mm layer height setting. The Block-6 block copolymer was synthesized via controlled radical polymerization using a reversible addition-fragmentation process described in detail in the previous work.[60] Briefly, the PSS-macro-RAFT precursor and the $PSS_{(1)}$-*b*-$PPEGMEA_{(6)}$ were synthesized using a two-step RAFT polymerization. After purification of the $PSS_{(1)}$-*b*-$PPEGMEA_{(6)}$, PEDOT was added onto the block copolymer via oxidative polymerization to make PEDOT:$PSS_{(1)}$-*b*-$PPEGMEA_{(6)}$ (Figure 2a). The 3-D printed molds were cleaned in a sonication bath for 10 min each using deionized water and isopropyl alcohol, successively. Once fully dried, the molds were cleaned in an air plasma cleaner for 5 min at 30 W and 250 mTorr to remove the excess contaminants from the mold surface. A mold release spray (Ease Release 200, Mann Release Technologies) was used to coat the surface of the molds before drop-casting 1 mL of filtered and degassed Block-6. The films were dried on a hotplate at

60 °C for 2.5 h. The molds were cooled down to room temperature before removing the films from the molds (Figure 2b). Finally, the electrical connections were fixed using copper wiring (36-G) and fast-drying silver paint (Ted Pella, Inc). This method produced sEMG electrodes with an area of $2.78 \pm 0.155$ cm$^2$ and a thickness of $41 \pm 3$ μm.

*Mechanical and Electrical Characterization of Block-6 sEMG Sensors*: The durability and stability of the Block-6 sEMG sensor films by measuring the cyclic piezoresistive response as well as the mechanical (tensile) properties using a linear actuator were quantified. Block-6 films used for mechanical and electronic testing were prepared using the methods described previously. To generate dog bone shaped samples, a mold ($l = 1.6$ cm, $w = 0.4$ cm, $h = 41$ μm) was 3D printed,treated and cast with 1 mL of Block-6 solution (0.27 g/100 mL PEDOT:PSS and 2.7 g/100 mL of PSS-b-PPEGMEA) For tensile tests, black electrical tape was wrapped around the ends of the dog bones to prevent fracture under the grips of the linear actuator. The dog bones were then placed in 3D printed grips connected to a Mark-10 Series 5 force gauge with 10 N maximum capacity all mounted on a Mark-10 motorized test stand. The samples were pulled until fracture at 1 mmmin$^{-1}$ and force-elongation data were collected. After fracture, the thickness of each dogbone was measured using a Dektak XT profilometer. The force-elongation data were then converted to stress–strain data using the geometry of each dog bone. The modulus was determined from the slope of the linear regime, and the linear elasticity (e.g., a proxy for intrinsic elasticity) was calculated as the strain at which the linear regime ended. For piezoresistive measurements, copper wires (36 G) were attached to the ends of each dogbone (underneath the black electrical tape) using carbon paint (Ted Pella, Inc) to ensure a good electrical connection between the wire and the film. These wires were connected to alligator clips attached to a Keithley 2601B Sourcemeter such that the resistance could be measured simultaneously using a custom written LabView program. For piezoresistive measurements, the linear actuator elongated the samples at a rate of 60 mmmin$^{-1}$ until a certain strain (5%, 10%, 15%, 20%, and 30%) was reached before allowing the film to return to its original position (i.e., 0% strain). These cyclic measurements were repeated for 400 cycles.

For electrical characterization, an electrochemical impedance spectroscopy was used to measure the electrode–skin and electrode–electrode impedance of the Block-6 electrodes in the range of 1 Hz to 100 kHz and was compared to the Ag/AgCl (RedDot, 3 M) electrodes, and commercial PEDOT:PSS (Clevios, prepared the same way as the Block-6 electrodes) with a potentiostat (Bio-Logic SP-200). The experiment was set up in a two-electrode configuration. A sinusoidal signal of 10 mV without any DC bias was supplied to the electrodes. All the electrodes were placed on the skin of the submandibular area and the impedance spectra were measured over 60 min. The Block-6 and Clevios electrode films had an area of $2.89 \pm 0.23$ cm$^2$ each and were separated by 2 cm. The Ag/AgCl electrodes had an area of 3.48 cm$^2$ (3 M Datasheet, 2560) and were separated by 6 cm. Lastly, the conductivities of the Block-6 films were measured with a four-point probe assembly connected to a Keithley 2400 source meter.

*Wireless Data Acquisition Using a PCB Board*: For a portable experiment setup, a custom PCB was designed with the capability of wireless data transfer of the strain and sEMG data to the desired client, a smartphone in the case (Figure 1e). The design contains programmable settings such as filtering, gain setting, and sampling rate for better flexibility. There were two main components on the PCB. The first one was MAX30001 (Maxim Integrated) which was the Analog Frontend (AFE) responsible for the data acquisition and processing of the data. The second one was CYW20736S (Cypress Semiconductor) which was a Bluetooth Low Energy (BLE)-enabled System-on-a-Chip (SoC)responsible for controlling the AFE and other Integrated Circuits on the PCB as well the full wireless communication with the smartphone. The PCB was powered by a 3.7 V (150 mAH) Li-ion battery that was attached to the backside of the board. A charging coil, LTC4124 (Analog Device), was also attached to the battery for wireless charging capability.

A firmware code was written and loaded into the SoC that managed all the BLE communications, the internal data storage, and the transfer from the AFE. For ease of access, a few predefined profiles were set up in the firmware that could be used to quickly set up a working link with the smartphone. The sEMG channel was set to have a sampling frequency of 512 Hz with a voltage gain of 20, and the strain channel to have a sampling frequency of 64 Hz and a voltage gain of 10. For the strain channel, an analog high-pass filter cutoff of 7.2 kHz was added, and a current source of 48 μA. The digital low pass and high pass filters were bypassed in both channels. To be able to support such a high bandwidth of data (in comparison to other common BLE use-case scenarios) and keep the data accurate (i.e., without dropping any samples), the data throughput by changing the connection interval, notification size, and only sending the necessary information in packets were maximized. Secondly, the internal FIFO memory of the AFE for temporary data storage was utilized and a burst mode was used to send the data to the SoC. The code and the interrupt cycle for the AFE were also set up in such a way that the sEMG and strain data were as time synchronous as possible barring the hardware latency coming from the AFE.

A smartphone with the "nRF Connect for Mobile" App (Nordic Semiconductor) was used to communicate and receive the data from this PCB. This application was a generic one for working with any BLE device. Once the communication link was set up and the data on the smartphone were received, a MATLAB script to clean up and decode the data was utilized. This script converted the information that was stored in notification packets into meaningful voltage samples and assigned a timestamp to each sample. These voltage samples were then finally fed into the ML model.

The stable connectivity range of the board once it was connected to the host was around 52 m and if it was not already connected then it was around 16 m. The battery on the PCB was able to last up to 15 h when it was fully charged. In order to keep the sensor–PCB interface compact and sturdy, a custom-designed USB-C connector on the board was used. This connector had two electrode cables for the sEMG sensor and two electrode cables for the strain gauge. The size of the whole assembled PCB including the battery was around 2.5 cm × 4.5 cm × 0.5 cm. This arrangement allowed to carry out the experiments in various environments with ease and without the need for any expensive data acquisition equipment.

*Human Subject Procedures*: A study involving a cohort of 10 healthy participants (ages between 21 and 34 years old; 6 female, 4 male) was carried out. Five of the ten participants were selected to walk while the other five were selected to cycle. The study was approved by the Internal Review Board at the University of California San Diego Human Research Protections Program (Project # 191950S). Participants signed informed consent forms prior to the study. Male subjects were instructed to shave their necks before coming to the study. Two Block-6 sEMG electrodes were symmetrically placed on the skin exterior to the hyoid muscles (mylohyoid and stylohyoid) in the submandibular region. The strain gauge was positioned in the middle of the throat, right under the laryngeal prominence. The long axis of the rectangular strain gauge was transverse to the neck. The PCB was attached to the participant's shoulder using tape. Tegaderm film was placed over the strain sensor and electrodes for prolonged adhesion.

The participants were either instructed to bike on a stationary bicycle or walk while they were given different volumes of water to swallow. Volume-controlled servings of water were given the participants, and they were asked to swallow it single attempt (i.e., no piecewise swallowing) on queue. Volumes from 10 to 30 mL in 5 mL increments were tested, repeating each volume 10 times. It was observed in previous work that 30 mL was about the maximum amount that participants can comfortably swallow, and the 10 mL was approximately the minimum volume where participants felt a difference from swallow of only saliva.

## Supporting Information

Supporting Information is available from the Wiley Online Library or from the author.

## Acknowledgments

B.P and T.R contributed equally to this work. This work was supported by the National Science Foundation award CBET-2223566 and a gift from

PepsiCo and the Gatorade Sports Sciences Institute. Additional support was provided by the member companies of the Center for Wearable Sensors in the Jacobs School of Engineering at the University of California, San Diego, including Dexcom, Gore, Honda, Huami, Instrumentation Laboratory, Kureha, Merck KGaA, Roche, Samsung, and Sony. L.B. acknowledges the support provided by the National Science Foundation Graduate Research Fellowship Program under Grant DGE-2038238. This work was performed in part at the San Diego Nanotechnology Infrastructure (SDNI), a member of the National Nanotechnology Coordinated Infrastructure, which is supported by the National Science Foundation (Grant ECCS-1542148). The visual abstract was partially created using BioRender.com. The authors would like to thank Prof. Tse Nga (Tina) Ng at UC San Diego for the helpful discussions.

## Conflict of Interest

The authors declare no conflict of interest.

## Data Availability Statement

Research data are not shared.

## Keywords

wireless epidermal sensors, nanostructures on graphene, PEDOT:PSS, surface-electromyography, machine learning, swallowing, exercise study

Received: November 2, 2022
Revised: December 21, 2022
Published online: January 18, 2023

[1] D. F. Roden, K. W. Altman, *Otolaryngol. Clin. North Am.* **2013**, *46*, 965.
[2] A. Eisbruch, M. Schwartz, C. Rasch, K. Vineberg, E. Damen, C. J. Van As, R. Marsh, F. A. Pameijer, A. J. M. Balm, *Int. J. Radiat. Oncol. Biol. Phys.* **2004**, *60*, 1425.
[3] L. Rofes, N. Vilardell, P. Clavé, *Neurogastroenterol. Motil.* **2013**, *25*, 278.
[4] K. A. Hutcheson, J. S. Lewin, D. A. Barringer, A. Lisec, G. B. Gunn, M. W. S. Moore, F. C. Holsinger, *Cancer* **2012**, *118*, 5793.
[5] B. R. Garon, T. Sierzant, C. Ormiston, *J. Neurosci. Nurs.* **2009**, *41*, 178.
[6] L. Sura, A. Madhavan, G. Carnaby, M. A. Crary, *Clin. Interventions Aging* **2012**, *7*, 287.
[7] N. Bhattacharyya, *Laryngoscope* **2015**, *125*, 746.
[8] N. Bhattacharyya, *Otolaryngol. – Head Neck Surg.* **2014**, *151*, 765.
[9] J. B. Palmer, K. V. Kuhlemeir, D. C. Tippett, C. Lynch, *Dysphagia* **1993**, *8*, 209.
[10] J. A. Logemann, *Manual for the Videofluorographic Study of Swallowing*, PRO-ED, Austin, TX **1993**.
[11] J. A. Logemann, *Otolaryngol. Head Neck Surg.* **1997**, *116*, 335.
[12] B. Martin-Harris, J. A. Logemann, S. McMahon, M. Schleicher, J. Sandidge, *Dysphagia* **2000**, *15*, 136.
[13] S. G. Hiss, G. N. Postma, *Laryngoscope* **2003**, *113*, 1386.
[14] B. Nicholls, C. S. Ang, K. Eiman, P. Siriaraya, S. Mirzaee Bafti, W.-H. Yeo, A. Tsanas, *Comput. Biol. Med.* **2022**, *149*, 106068.
[15] J. M. Fontana, M. Farooq, E. Sazonov, *Detection and Characterization of Food Intake by Wearable Sensors*, Elsevier Inc, Cambridge, MA **2020**.
[16] M. Farooq, E. Sazonov, *Sensors* **2016**, *16*, 1067.
[17] K. Matsuo, J. B. Palmer, *Phys. Med. Rehabil. Clin. N Am.* **2008**, *19*, 691.
[18] C. Ertekin, M. Pehlivan, I. Aydoğdu, M. Ertaşl, B. Uludağ, G. Çlelebi, Z. Çlolakoğlu, A. Sağduyu, N. Yüceyar, *Muscle Nerve* **1995**, *18*, 1177.
[19] B. Jones, *Normal and Abnormal Swallowing*, Springer, New York, NY **2003**.
[20] S. M. Shaw, R. Martino, *Otolaryngol. Clin. North Am.* **2013**, *46*, 937.
[21] C. Ertekin, I. Aydogdu, *Clin. Neurophysiol.* **2003**, *114*, 2226.
[22] K. M. Hiiemae, J. B. Palmer, *Dysphagia* **1999**, *14*, 31.
[23] C. Schultheiss, T. Schauer, H. Nahrstaedt, R. O. Seidl, *Sci. World J.* 1–7, **2014**, *2014*.
[24] Y. Koyama, N. Ohmori, H. Momose, S. Ichi Yamada, H. Kurita, *J. Dent. Sci.* **2022**, *16*, 1185.
[25] L. Reimers-Neils, J. Logemann, C. Larson, *Dysphagia* **1994**, *9*, 101.
[26] Y. Fu, J. Zhao, Y. Dong, X. Wang, *Sensors***2020**, *20*, 3651.
[27] B. Nicholls, C. S. Ang, C. Efstratiou, Y. Lee, W. H. Yeo, *2017 IEEE International Conference on Pervasive Computing and Communications Workshops, PerCom Workshops 2017*, **2017**, p. 413.
[28] G. Constantinescu, J. W. Jeong, X. Li, D. K. Scott, K. I. Jang, H. J. Chung, J. A. Rogers, J. Rieger, *Med. Eng. Phys.* **2016**, *38*, 807.
[29] S. Velasco-Bosom, N. Karam, A. Carnicer-Lombarte, J. Gurke, N. Casado, L. C. Tomé, D. Mecerreyes, G. G. Malliaras, *Adv. Healthcare Mater.* **2021**, *10*, 2100374.
[30] D. Pani, A. Dessi, J. F. Saenz-Cogollo, G. Barabino, B. Fraboni, A. Bonfiglio, *IEEE Trans. Biomed. Eng.* **2016**, *63*, 540.
[31] J. Ouyang, *SmartMat* **2021**, *2*, 263.
[32] K. Wang, U. Parekh, T. Pailla, H. Garudadri, V. Gilja, T. N. Ng, *Adv. Healthcare Mater.* **2017**, *6*, 1700552.
[33] L. Zhang, K. S. Kumar, H. He, C. J. Cai, X. He, H. Gao, S. Yue, C. Li, R. C. S. Seet, H. Ren, J. Ouyang, *Nat. Commun.* **2020**, *11*, 1700552.
[34] Y. Zhao, S. Zhang, T. Yu, Y. Zhang, G. Ye, H. Cui, C. He, W. Jiang, Y. Zhai, C. Lu, X. Gu, N. Lie, *Nat. Commun.* **2021**, *12*, 4880.
[35] J. Cao, X. Yang, J. Rao, A. Mitriashkin, X. Fan, R. Chen, H. Cheng, X. Wang, J. Goh, H. L. Leo, J. Ouyang, *ACS Appl. Mater. Interfaces* **2022**, *14*, 39159.
[36] E. A. Clancy, E. L. Morin, R. Merletti, *J. Electromyogr. Kinesiology* **2002**, *12*, 1.
[37] R. H. Chowdhury, M. B. I. Reaz, M. A. Bin Mohd Ali, A. A. A. Bakar, K. Chellappan, T. G. Chang, *Sensors* **2013**, *13*, 12431.
[38] M. K. Kim, C. Kantarcigil, B. Kim, R. K. Baruah, S. Maity, Y. Park, K. Kim, S. Lee, J. B. Malandraki, S. Avlani, A. Smith, S. Sen, M. Alam, G. Malandraki, C. H. Lee, *Sci. Adv.* **2019**, *5*.
[39] J. Ramírez, D. Rodriquez, F. Qiao, J. Warchall, J. Rye, E. Aklile, A. S.-C. Chiang, B C. Marin, P P. Mercier, C. K. Cheng, K A. Hutcheson, E H. Shinn, D J. Lipomi, *ACS Nano* **2018**, *12*, 5913.
[40] C. Schultheiss, T. Schauer, H. Nahrstaedt, R. O. Seidl, *Eur. Arch. Otorhinolaryngol.* **2013**, *270*, 2149.
[41] E. Roh, B. U. Hwang, D. Kim, B. Y. Kim, N. E. Lee, *ACS Nano* **2015**, *9*, 6252.
[42] B. U. Hwang, J. H. Lee, T. Q. Trung, E. Roh, D. Il Kim, S. W. Kim, N. E. Lee, *ACS Nano* **2015**, *9*, 8801.
[43] S. H. Zhang, F. X. Wang, J. J. Li, H. D. Peng, J. H. Yan, G. B. Pan, *Sensors* **2017**, *17*, 2621.
[44] Y. Sakaue, T. Shimizu, M. Matsushima, M. Matsuura, K. Takahashi, K. Asahara, S. Okada, M. Makikawa, *Proceedings of the Annual International Conference of the IEEE Engineering in Medicine and Biology Society*, EMBS, **2013**, p. 612.
[45] Y. Zhu, Y. Hu, P. Zhu, T. Zhao, X. Liang, R. Sun, C. P. Wong, *New J. Chem.* **2017**, *41*, 4950.
[46] Y. Huang, Y. Zhao, Y. Wang, X. Guo, Y. Zhang, P. Liu, C. Liu, Y. Zhang, *Smart Mater. Struct.* **2018**, *27*, 035013.
[47] Y. Koyama, N. Ohmori, H. Momose, E. Kondo, S. Ichi Yamada, H. Kurita, *J. Dent. Sci.* **2021**, *16*, 160.
[48] J. Lee, C. M. Steele, T. Chau, *Artif. Intell. Med.* **2011**, *52*, 17.
[49] Y. R. Jeong, J. Kim, Z. Xie, Y. Xue, S. M. Won, G. Lee, S. W. Jin, S. Y. Hong, X. Feng, Y. Huang, J. A. Rogers, J. S. Ha, *NPG Asia Mater.* **2017**, *9*, e443.

[50] J. Ramírez, D. Rodriquez, A. D. Urbina, A. M. Cardenas, D. J. Lipomi, *ACS Appl. Nano Mater.* **2019**, *2*, 2222.
[51] B. Polat, L. L. Becerra, P. Y. Hsu, V. Kaipu, P. P. Mercier, C. K. Cheng, D. J. Lipomi, *ACS Appl. Nano Mater.* **2021**, *4*, 8126.
[52] J. Ramírez, A. D. Urbina, A. T. Kleinschmidt, M. Finn, S. J. Edmunds, G. L. Esparza, D. J. Lipomi, *Nanoscale* **2020**, *12*, 11209.
[53] B. C. Marin, S. E. Root, A. D. Urbina, E. Aklile, R. Miller, A. V. Zaretski, D. J. Lipomi, *ACS Omega* **2017**, *2*, 626.
[54] M. Huang, T. A. Pascal, H. Kim, W. A. Goddard, J. R. Greer, *Nano Lett.* **2011**, *11*, 1241.
[55] A. D. Smith, F. Niklaus, A. Paussa, S. Vaziri, A. C. Fischer, M. Sterner, F. Forsberg, A. Delin, D. Esseni, P. Palestri, M. Östling, M. C. Lemme, *Nano Lett.* **2013**, *13*, 3237.
[56] N. J. G. Couto, D. Costanzo, S. Engels, D. K. Ki, K. Watanabe, T. Taniguchi, C. Stampfer, F. Guinea, A. F. Morpurgo, *Phys. Rev. X* **2014**, *4*, 041019.
[57] R. Skomski, P. A. Dowben, M. Sky Driver, J. A. Kelber, *Mater. Horiz.* **2014**, *1*, 563.
[58] J. Hicks, A. Tejeda, A. Taleb-Ibrahimi, M. S. Nevius, F. Wang, K. Shepperd, J. Palmer, F. Bertran, P. Le Fèvre, J. Kunc, W. A. de Heer, C. Berger, E. H. Conrad, *Nat. Phys.* **2013**, *9*, 49.
[59] O. Jin Young, S. Kim, H. K. Baik, U. Jeong, *Adv. Mater.* **2016**, *28*, 4455.
[60] R. Blau, A. X. Chen, B. Polat, L. L. Becerra, R. Runser, B. Zamanimeymian, K. Choudhary, D. J. Lipomi, *ACS Appl. Mater. Interfaces* **2022**, *14*, 4823.
[61] A. Elschner, S. Kirchmeyer, L. Wilfried, U. Merker, K. Reuter, *PEDOT: Principles and Applications of an Intrinsically Conductive Polymer*, CRC Press, Boca Raton **2010**.
[62] L. Groenendaal, F. Jonas, D. Freitag, H. Pielartzik, J. R. Reynolds, *Adv. Mater.* **2000**, *12*, 481.
[63] S. Kirchmeyer, K. Reuter, *J. Mater. Chem.* **2005**, *15*, 2077.
[64] H. Shi, C. Liu, Q. Jiang, J. Xu, *Adv. Electron. Mater.* **2015**, *1*, 1500017.
[65] Y. Wen, J. Xu, *J. Polym. Sci., Part A: Polym. Chem.* **2017**, *55*, 1121.
[66] K. A., K. A., *J. Mater. Sci. Eng.* **2016**, *5*, 1000254.
[67] C. E. Stepp, *J. Speech Hear. Res.* **2012**, *55*, 1232.
[68] M. Poorjavad, S. Talebian, N. Nakhostin Ansari, Z. Soleymani, *Iran J. Med. Sci.* **2017**, *42*, 194.
[69] D. Stegeman, H. Hermens, *Enschede Roessingh Res. Dev.*, **2007**, p. 108.
[70] H. Drucker, C. J. C. Surges, L. Kaufman, A. Smola, V. Vapnik, *Adv. Neural Inf. Process. Syst.* **1997**, *1*, 155.
[71] Y. An, C. Ji, Y. Li, J. Wang, X. Zhang, Y. Huang, *Med. Phys.* **2017**, *44*, 1402.